# 19.3 Mobile Radar Observations of Tornadic Supercells with Multiple Rear-Flank Gust Fronts

JAMES MARQUIS*, YVETTE RICHARDSON,
*Department of Meteorology, Pennsylvania State University, University Park, PA*
JOSHUA WURMAN,
*Center for Severe Weather Research, Boulder, CO*
PAUL MARKOWSKI,
*Department of Meteorology, Pennsylvania State University, University Park, PA*
DAVID DOWELL
*National Center for Atmospheric Research, Boulder, CO*

## 1. Introduction

The structure of classic mature supercell storms has been deduced in past studies using visual observations, coarse resolution radar data, and idealized model simulations (e.g. Fig.7 in Lemon and Doswell 1979). In such models, low-level kinematic structures include an updraft that is surrounded by downdrafts on the rear-flank and forward-flank of the storm. At low-levels, the updraft usually is horseshoe-shaped, arcing outward from beneath the primary mid-level updraft along the interface between evaporatively cooled outflow air on the rear-flank of the storm and the buoyant environmental air (rear-flank gust front). A low-level mesocyclone is located where the primary updraft and rear-flank downdraft meet, and if a tornado is to form, it will usually occur in this area of strong storm-scale vorticity. Tornadogenesis occurs near the time of occlusion between the rear-flank and forward-flank gust fronts and is accompanied by a smaller-scale occlusion downdraft. Although the specific role of the rear-flank downdraft in the tornadogenesis process has yet to be validated by fine-resolution observations of combined wind and thermodynamic data, it is speculated that this downdraft may serve as a source of horizontal, baroclinically-generated vortex rings that become tilted into the vertical at the interface between updraft and downdraft (Straka et al. 2007; Markowski et al. 2008). The tornado is assumed to persist until it loses its source of angular momentum or until negatively buoyant outflow air surrounds the tornado and cuts off the supply of positively buoyant environmental air to the primary updraft. This choking of the updraft ends the contraction of near-surface angular momentum.

Data collected in a tornadic supercell by the Doppler on Wheels (DOW) radars have shown the presence of multiple rear-flank gust fronts occurring simultaneously, with a wind shift line visible in the outflow air behind a preceding rear-flank gust front (Wurman et al. 2007). At least one numerical simulation also produced this dual gust front structure (Adlerman 2003). In addition, mobile mesonet observations have indicated the presence of secondary surface wind shifts behind the main rear-flank gust front, with accompanying temperature perturbations (Finley and Lee 2004 and Lee et al. 2004). The source of these secondary gust fronts is not clear, nor is their role in the tornadogenesis process or in tornado maintenance. For example, these secondary downdrafts could represent an injection of vortex rings at low-levels, possibly aiding tornadogenesis or tornado maintenance, but, on the other hand, they may represent injections of cold air that would quickly surround the tornado and disrupt the vortex.

This paper will discuss the morphology, retrieved temperature gradients, and evolution of the multiple gust front configurations observed in several tornadic supercells observed by the Doppler on Wheels radars. These data are presently being analyzed in the context of tornado maintenance; therefore, a particular emphasis is placed on the discussion of multiple gust fronts as they relate to tornado duration and strength.

## 2. Data

A combination of dual- and single-Doppler data collected in three supercell storm intercepts by the DOWs are used to examine the structure of multiple rear-flank gust fronts in the vicinity of tornadoes. These three cases include storms intercepted on 5 June 2001 near Argonia, KS (Dowell et al. 2002); 30 April 2000 near Crowell, TX (Marquis et al. 2008); and 22 May 2004 near Orleans, NE.

Dual-Doppler syntheses of the three-dimensional wind field are produced using an upward iterative calculation of the mass continuity equation. Objective analysis of single-Doppler data used in the wind syntheses are performed with a Barnes smoothing parameter and grid spacing as suggested by Pauley and Wu (1990), Koch et al. (1983), and Trapp and Doswell (2000). A two-pass smoothing was performed, with gamma equal to 0.3 (Majcen et al. 2008). The Barnes response function for each case has a value of 0.65 or greater for spatial scales of 1km, and $> 0.95$ for scales larger than 2 km; therefore, gust front features are well resolved, and the scales associated with the tornado cyclone are marginally resolved.

Analyses based on data assimilation of single-Doppler DOW radial velocity observations are used to examine multiple gust front structures in the 5 June 2001 case. The assimilations are

**Corresponding author address*: James Marquis, Department of Meteorology, Pennsylvania State University, 503 Walker Building, University Park, PA 16802; *e-mail*: jmarquis@met.psu.edu.

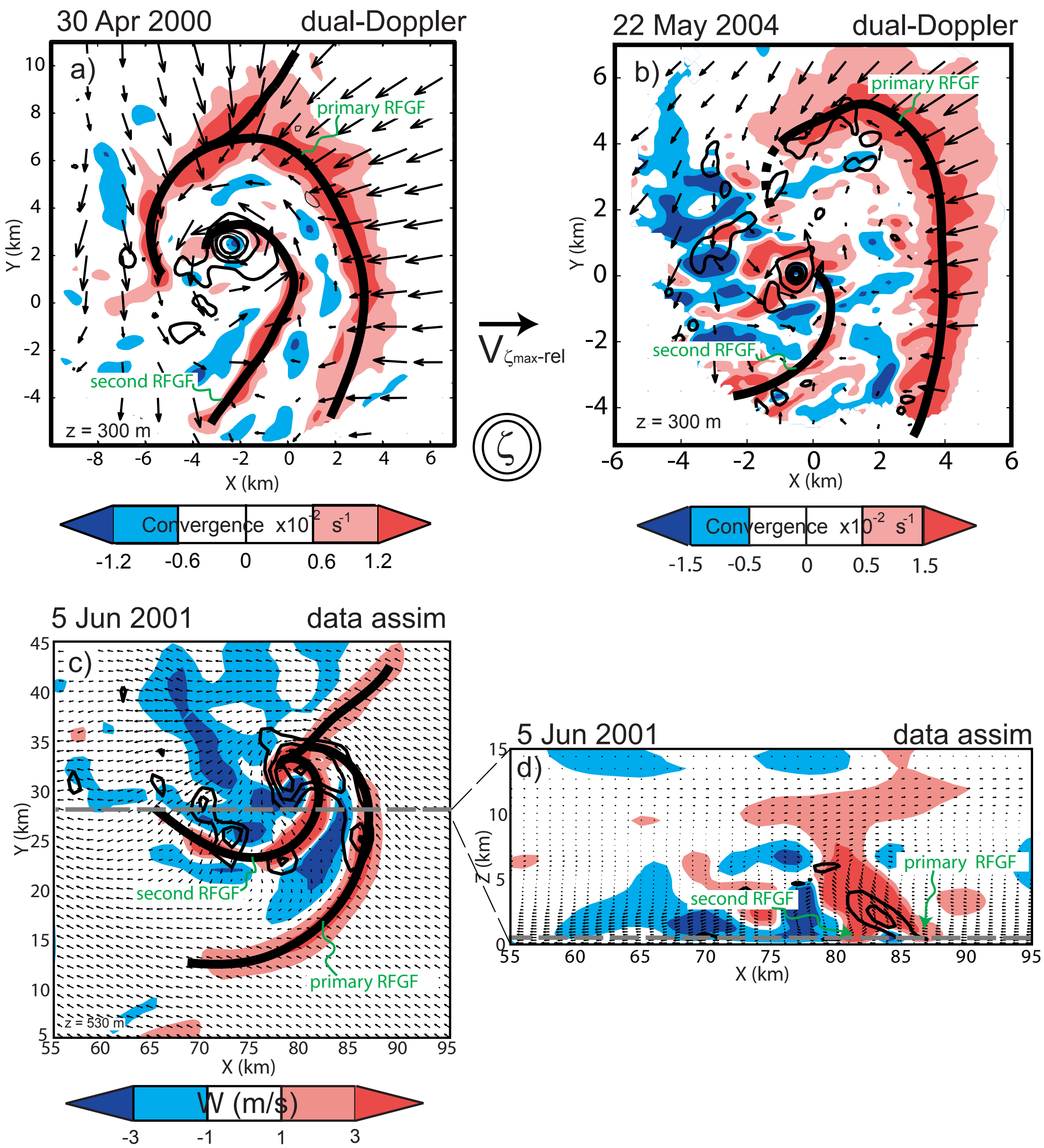


FIG. 1. a) Dual-Doppler convergence (shaded), positive vertical vorticity (contoured), and horizontal wind relative to the vorticity maximum (vectors) in the x-y plane at z = 300 m AGL and 2108 UTC on 30 April 2000. b) Same as a) but at 2304 UTC on 22 May 2004. c) Ensemble mean: vertical motion (shaded), positive vertical vorticity (contoured), and storm-relative horizontal winds (vectors) in an x-y plane at z = 530 m AGL and 0036 UTC on 5 June 2001 produced by assimilation of DOW3 velocities into the WRF model with the ensemble Kalman filter method. d) An x-z cross section along the gray dashed line in c). Primary and secondary gust fronts are illustrated with bold black lines in each panel. Wind vectors are valid for the grid location at the end of their tails.

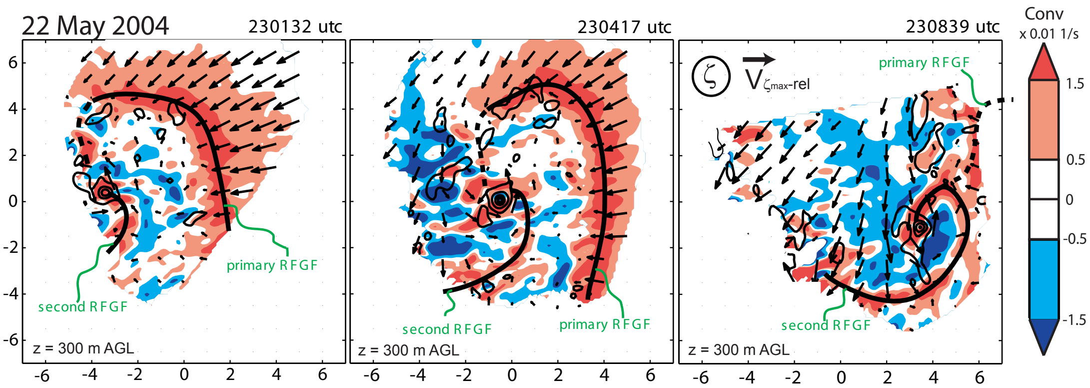


FIG. 2. Dual-Doppler convergence (shaded), positive vertical vorticity (contoured), and horizontal wind relative to the vorticity maximum (vectors) in the x-y plane at z = 300 m AGL and a) 230132, b) 230417, and c) 230839 UTC on 22 May 2004. Primary and secondary gust fronts are illustrated with bold black lines in each panel. Wind vectors are valid for the grid location at the end of their tails.

performed via the ensemble Kalman filter technique (e.g. Snyder and Zhang 2003) using the WRF cloud model. Gaussian noise is added to the horizontal wind vectors, temperature, and dew point temperature every five minutes in order to maintain ensemble spread throughout the experiment run time (Dowell and Wicker 2008).

## 3. Kinematics

Multiple gust front configurations are observed with the DOW radars (Fig.1), with each case showing a prominent low-level convergence (or w > 0 as in Fig.1c) band encircling the vorticity maximum and leading an area of low-level divergence (or w < 0). The position and shape of this easternmost convergence band is consistent with the presence of a rear-flank gust front boundary (hereafter RFGF) that is commonly found at the interface between environmental inflow and storm outflow (hereafter primary RFGF). Also found in each example is a secondary convergence band in the divergent and/or descending outflow air behind the primary RFGF. These secondary bands, termed here secondary RFGFs, spiral outward cyclonically (southward) from a point near the surface vorticity maximum, in accordance with the highly curved gusting outflow winds south-southwest of the tornado. The gusting outflow winds behind (west of) the secondary RFGFs are stronger than the outflow winds east of them, with a $\Delta |V| \approx$ 10-25 m/s, consistent with wind shifts observed with mobile mesonet instruments in some multiple RFD surge events (Finley and Lee 2004, Lee et al. 2004). The limited vertical extent of the data precludes our ability to determine the depth of the secondary convergence swaths using dual-Doppler syntheses alone. However, the data assimilation results for the 5 June 2001 case show that the vertical velocity associated with the secondary gust front merges with that associated with the primary gust front at the base of the storm updraft at a height of 2-3 km AGL within a few kilometers range of the tornado (Fig.1d).

We observe the motion of the multiple RFGFs over 10-15 minute periods in the 22 May 2004 and 30 April 2000 storms. During these time periods, the secondary RFGFs cyclonically wrap around the low-level vorticity maximum (e.g.

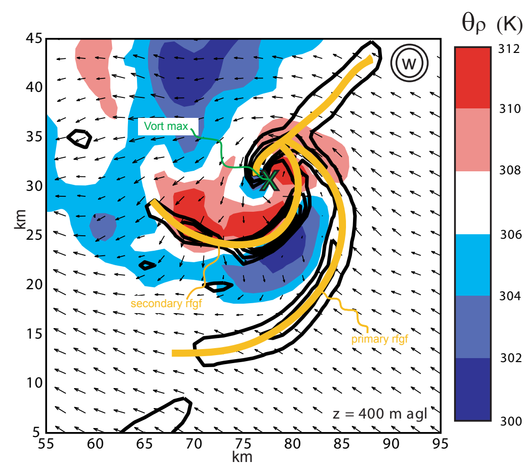


FIG. 3. Ensemble mean: vertical motion (w = 1, 3, 5, 7 m/s contours), density potential temperature (shaded), and storm-relative horizontal winds (vectors) in an x-y plane at z = 400 m AGL and 0036 UTC on 5 June 2001 produced by assimilation of DOW3 velocities into the WRF model with the ensemble Kalman filter method. Primary and secondary gust fronts are illustrated with bold orange lines. Wind vectors are valid for the grid location at the end of their tails.

Fig.2) in a manner presumed to be similar to that of the primary RFGF. The portion of the secondary RFGF in close proximity to the vorticity maximum spirals around it most rapidly. Comparitively, the portion of the secondary RFGF farther south maintains a more steady location relative to the vorticity maximum and the primary RFGF. The forward (cyclonic, outward-spiraling) motion of the secondary RFGFs rapidly increases with the development of strong low-level divergence behind them, particularly in a location approximately 2km south through east of each vorticity maximum. This suggests that newly forming downdraft localized within a few kilometers of the tornado may play a role in the motion of the secondary gust front, similar to the manner in which the primary RFGF follows the leading edge of the rear-flank downdraft in the depiction of a classic supercell (Lemon and Doswell 1979).

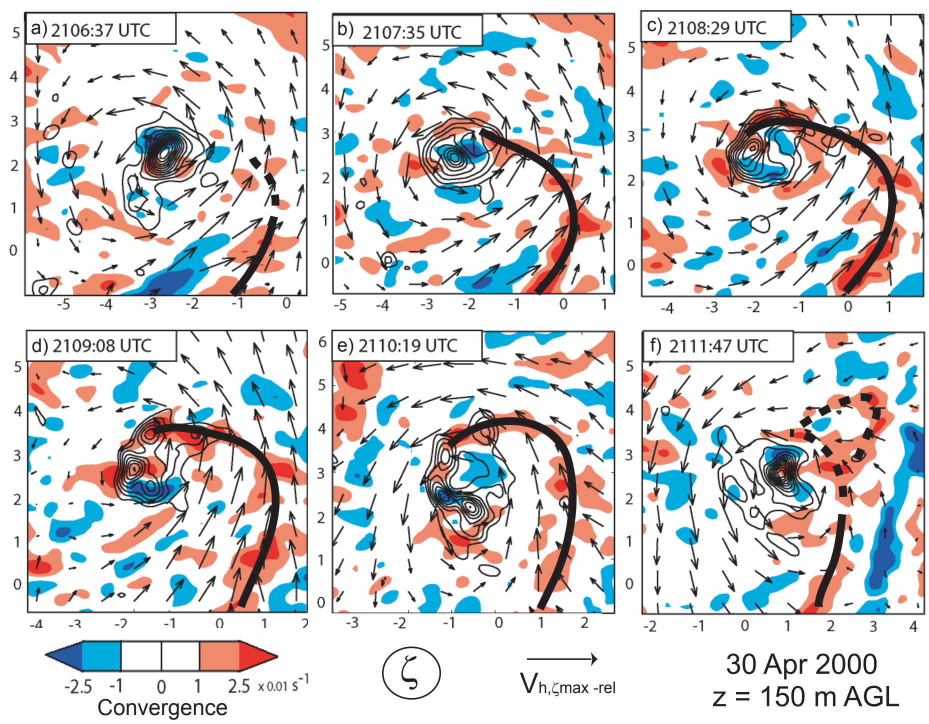


FIG. 4. Dual-Doppler convergence (shaded), positive vertical vorticity (contoured), and horizontal wind relative to the vorticity maximum (vectors) in the x-y plane at z = 150 m AGL and a) 210637, b) 210735, c) 210829, d) 210908, e) 211019, f) 211147 UTC on 30 April 2000. Convergence along the secondary gust front is illustrated with a bold black line in each panel; dashed lines indicate uncertainty in its position. Wind vectors are valid for the grid location at the end of their tails. Adapted from Marquis et al. 2008.

The cause of the secondary downdrafts within the rear-flank downdraft region in these cases is not known although they are consistent with an occlusion downdraft thought to form as low-level rotation exceeds that aloft (Rotunno and Klemp 1985). In the 5 June 2001 case, the secondary RFGF develops during the DOW deployment and is not observed for a significant time in its mature state. However, the developing secondary RFGF moves toward the east at a speed similar to that the primary RFGF. A strengthening downdraft is found east and south of the tornado at the same time that the second RFGF is developing, further implying a relationship between the second RFGF and a rear-flank downdraft surge.

## 4. Thermodynamics

Finley and Lee (2004) and Lee et al. (2004) measured thermodynamic data at the surface using moblie mesonets in multiple RFD surges in a few supercells. They found variable $\theta_v$ and $\theta_e$ perturbations associated with each RFD surge (i.e. behind each RFGF); some RFD surges were cooler than others in the same storm, and some of the RFD surges were warmer than preceding ones. In-situ thermodynamic measurements are not available for the present study. However, temperature fields are recovered for the 5 June 2001 case by assimilating the radar data into the WRF model using the ensemble Kalman filter method. Although caution must be exercised in the interpretation of the resulting fields, as they are produced by a statistical relationship with the assimilated DOW radial velocities rather than by a direct dynamical relationship, the resulting pattern of $\theta$ evolves smoothly in time and matches well with the spatial distribution of the two RFGFs, which perhaps qualitatively verifies the legitimacy of the results.

In this storm, the low-level (z $\approx$ 500 m AGL) $\theta_\rho$ (Emanuel 1994) field (e.g. Fig.3) indicates that the outflow immediately behind the primary RFGF is 2-6 K cooler than the environmental air. In contrast, values of $\theta_\rho$ behind the second RFGF are as much as 2-4 K warmer than the environmental air and, thus, are 4-10 K warmer than the preceding outflow air. This pattern is consistent with the variable values of $\Delta\theta_v$' behind sequential RFGFs shown in Finley and Lee (2004), Lee et al. (2004), and in the Dimmitt, TX supercell (Fig.7 in Markowski et al. 2002). The warmer outflow air behind the second RFGF might suggest that the RFD surge causing it was not formed by evaporatively chilled descending air in this storm.

## 5. Relationship with tornado behavior

Preliminary results offer some evidence that the observed secondary RFGF features play a role in tornado behavior. An approximately 5-minute sequence of dual-Doppler data collected near the ground (z $\approx$ 150 m AGL) in the 30 April 2000 storm shows an interesting interaction between the tornado-cyclone and a secondary RFGF (Fig.4). During this sequence, a generally symmetric vertical vorticity field with one distinct vorticity maximum (Fig.4a) transitions into a vortex-ring structure (Fig.4e) with isolated maxima on its western hemisphere and an annulus of convergence surrounding divergence near its core. This structure closely resembles the conceptual model of a multiple-vortex tornado, but with an asymmetric distribution of vorticity about its center. During this transition in tornado structure, the expanding asymmetric vortex ring is connected to the convergence band of the secondary RFGF to the north/northeast of the ring center. Therefore, the asymmetric vorticity pattern appears to be tied to the surge of outflow air behind the second RFGF that causes it to wrap around the low-level center of rotation. By the end of the sequence (Fig.4f), the multi-vortex structure is replaced with a smaller, isolated vorticity maximum whose single-Doppler estimated peak velocity weakens over the next few minutes.

In the 5 June 2001 case, between 0030 and 0040 UTC, vertical motion along the developing second RFGF (south of the vorticity maximum at z = 500 m AGL) builds northward and makes contact with the primary RFGF and FFGF just west of the original occlusion point (Fig.1c). The tornado is located approximately 5-7 km from the first occlusion point and 3-4 km from the second (new) occlusion point; therefore, the tornado is more directly influenced by the warmer air behind the second RFGF than the cooler air behind the first RFGF. Between 0034 and 0040 UTC, the tornado, as observed with single-Doppler data, is decreasing in intensity. The fact that relatively warm outflow surrounds the dying tornado implies that the presence of positively buoyant air at low-levels is not sufficient for tornado maintenance. We currently are investigating the role, if any, of the RFD surge (behind the second RFGF) in tornado demise. The RFGFs also influence the overall low-level mesocyclone as low-level vertical vorticity is increasing between the two occlusion points in the final few analysis times (e.g. $x$ = 82 km, $y$ = 31 km in Fig.1c) but is weakening west of the occlusion point of the secondary RFGF. This indicates the secondary RFGF, which seems to be replacing the primary RFGF, is directly involved with a cyclic mesocyclogenesis event.

In the 22 May 2004 case, the near-ground peak tangential velocity of the tornado increases while its core diameter decreases (implying a continuous contraction of angular momentum), consistent with the dual-Doppler syntheses that indicate a collocation of low-level convergence with tornadic vertical vorticity. This enhanced convergence is associated with the secondary gustfront as it wraps around the tornado but does not clearly connect to the primary RFGF (Fig.2b). Thus, the behavior of this tornado is almost certainly affected by the behavior of the secondary RFGF. The occlusion of the second RFGF with the primary RFGF appears to occur at the end of the DOW deployment. Unfortunately, the dissipation of the tornado is not observed by the DOWs, so we are unable to test the hypothesis that tornado demise occurs after the occluding second RFGF weakens the supply of low-level vorticity and/or convergence.

## 6. Summary

Three-dimensional wind fields produced in at least three tornadic storms observed by the Doppler on Wheels radars show evidence of multiple rear flank gust fronts. In each case, secondary rear-flank gust fronts are observed to wrap cyclonically around the tornadoes behind a more stationary (relative to the tornado) preceding rear-flank gust front. Thermodynamic information is retrieved in one case by assimilating radar velocities into a simulated supercell, and these results indicate varied

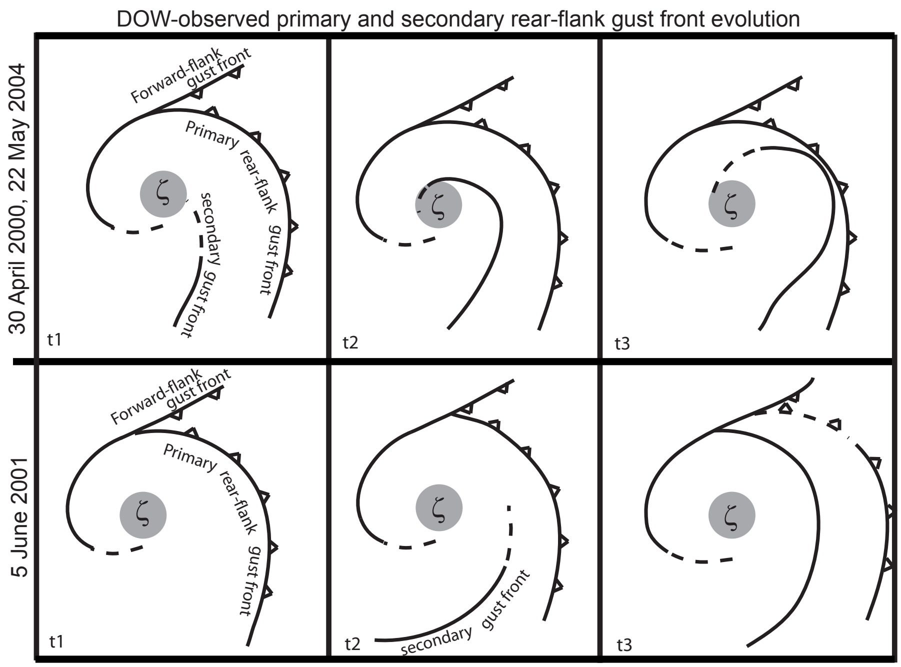


FIG. 5. Schematic illustration of the evolution of the primary and secondary rear-flank gust fronts at low-levels in the 30 April 2000 and 22 May 2004 storms (top), and the 5 June 2001 storm (bottom). The bold black lines trace the convergence swaths along each gust front; dashed bold lines indicate uncertainty in the subjective location of the gust fronts. The storm-scale low-level vertical vorticity in which each tornado is imbedded in shaded in each panel.

$\theta_\rho$ perturbations behind each of the gust fronts, consistent with some insitu surface observations of multiple rear-flank downdraft surges (Finley and Lee 2004 and Lee et al. 2004).

The multiple gust front structures are currently being examined in the context of tornado maintenance. The present cases suggest that the behavior of some of the observed tornadoes is affected by the evolution of secondary rear flank gust fronts and their associated pattern of low-level horizontal convergence/divergence. As such, tornado maintenance may be affected by a feature of the storm that develops and evolves well after the original wave of outflow air surrounds it (Fig 5).

There are several aspects of the observed multiple gust front structures that are presently unclear, including:

1. What are the dynamics processes relevant to the production of secondary rear flank gust fronts and their associated rear-flank downdraft surges? Are the formation mechanisms the same in all storms?
2. Are multiple gust front structures common to tornadic and non-tornadic supercell storms? Are they caused by tornadoes?
3. Do the dynamics processes that cause multiple gust fronts commonly affect the temperature structure of the outflow air?
4. In what situations do multiple gust front structures adversely or advantageously affect tornado strength?

If future studies can answer these questions, then we are likely to have a much more complete understanding of tornadic storm evolution. High-resolution data collected in the upcoming VORTEX 2 experiment and examined via dual-Doppler or data assimilation methods may be able to provide answers to these questions.

*Acknowledgments.* This project is funded by NSF grants ATM-0437512, ATM-0437505, ATM-0801035, and ATM-0801041. We would like to thank Curtis Alexander, Paul Robinson, Mario Majcen, Jeff Frame, Kent Knopfmeier, and Ryan Hastings for data and code support, and for analysis interpretation; and the ROTATE crews of the 2000, 2001, and 2004 years for the data collection itself.

REFERENCES

Adlerman, E.J., 2003: Numerical Simulations of Cyclic Storm Behavior: Mesocyclogenesis and Tornadogenesis. Ph.D. dissertaiton, University of Oklahoma, 217 pp. [Available form School of Meterology, University of Oklahoma, 100 East Boyd, Suite 1310, Norman, OK 73019.]

Barnes, S. L., 1964: A technique for maximizing details in numerical weather map analysis. *J. Appl. Meteor.*, **3**, 396–409.

Browning, K. A., 1964: Airflow and precipitation trajectories within severe local storms which travel to the right of the winds. *J. Atmos. Sci.*, **21**, 634–639.

Dowell, D.C., Y.P. Richardson, and J.M. Wurman, 2002: Observations of the Formation of Low-Level Rotation: The 5 June 2001

Sumner County, Kansas Tornado. *Preprints, 21st Conf. on Severe Local Storms*, San Antonio, Texas. Amer. Meteor. Soc., 12.3.

Dowell, D.C., L.J. Wicker 2008: Additive Noise for Storm-Scale Ensemble Forecasting and Data Assimilation. *J. Atmos. Oceanic Tech. in press*.

Emanuel, K.A., 1994: *Atmospheric Convection*. Oxford University Press, 161 pp.

Finley, C.A. and B.D. Lee, 2004: High Resolution Mobile Mesonet Observations of RFD Surges in the June 9 Basset, Nebraska Supercell During Project Answers 2003. *Preprints, 22nd Conf. on Severe Local Storms*, Hyannis, Mass, Amer. Meteor. Soc., 11.3.

Koch, S.E., M. desJardins, and P.J. Kocin, 1983: An Interactive Barnes Objective Map Analysis Scheme for Use with Satellite and Conventional Data. *J. Appl. Meteor.*, **22**, 1487-1503.

Lee, B.D., C.A. Finley, and P. Skinner, 2004: Thermodynamic and Kinematic Analysis of Multiple RFD Surges for the 24 June 2003 Manchester, South Dakota Cyclic Tornadic Supercell During Project Answers 2003. *Preprints, 22nd Conf. on Severe Local Storms*, Hyannis, Mass., Amer. Meteor. Soc., 11.2.

Lemon, L. R., and C.A. Doswell, 1979: Severe Thunderstorm Evolution and Mesocyclone Structure as Related to Tornadogenesis. *Mon. Wea. Rev.*, **107**, 1184-1197.

Majcen, M., P. Markowski, Y. Richardson, D. Dowell, J. Wurman 2008: Multi-pass objective analyses of Doppler radar data. *J. Atmos. Oceanic Tech. in press*.

Markowski, P., E. Rasmussen, R. Davies-Jones, Y. Richardson, and R.J. Trapp, 2008: Vortex Lines within Low-level Mesocyclones Obtained from Pseudo-Dual-Doppler Radar Observations. *Mon. Wea. Rev.*, **136**, 3513-3535.

Markowski, P.M., J. M. Straka, and E. N. Rasmussen, 2002: Direct surface thermodynamic observations within the rear-flank downdrafts of nontornadic and tornadic supercells.*Mon. Wea. Rev.*, **130**, 1692-1721.

Marquis, J., Y. Richardson, J. Wurman, P. Markowski, 2008: Single- and Dual-Doppler Analysis of a Tornadic Vortex and Surrounding Storm-Scale Flow in the Crowell, Texas, Supercell of 30 April 2000. *Mon. Wea. Rev. in press*.

Pauley, P. M., and X. Wu, 1995: The theoretical, discrete, and actual response of the Barnes objective analysis scheme for one- and two-dimensional fields. *Mon. Wea. Rev.*, **118**, 1145–1163.

Trapp, R. J.,and C. A. Doswell, 2000: Radar objective analysis. *J. Atmos. Oceanic Tech.*, **117**, 105–120.

Rotunno, R., and J.B. Klemp, 1985: On the Rotation and Propogation of Simulated Supercell Thunderstorms. *J. Atmos. Sci.*, **42**, 271–292.

Snyder, C., and F. Zhang, 2003: Assimilation of Simulated Doppler Radar Observations with an Ensemble Kalman Filter. *Mon. Wea. Rev.*, **131**, 1663-1677.

Straka, J.M., E.N. Rasmussen, R.P. Davis-Jones, and P.M. Markowski, 2007: An Observational and Idealized Numerical Examination of Low-level Counter-rotating Vortices Toward the Rear Flank of Supercells. *Electron. J. Severe Storms Meteor.*, **2**, 1–22.

Wurman, J., Y. Richardson, C. Alexander, S. Weygandt, and P.F. Zhang, 2007: Dual-Doppler and Single-Doppler Analysis of a Tornadic Storm Undergoing Mergers and Repeated Tornadogenesis. *Mon. Wea. Rev.*, **135**, 736-758.